

Article

# Completion of Crystallographic Data for the Series of 4-Halogenated-1*H*-pyrazoles: Crystal Structure Determination of 4-Iodo-1*H*-pyrazole and Spectroscopic Comparison

 Kelly L. Rue, Susana Herrera, Indranil Chakraborty, Alexander M. Mebel \* and Raphael G. Raptis \* 

Department of Chemistry and Biochemistry, Florida International University, Miami, FL 33199, USA; krue001@fiu.edu (K.L.R.); sherr058@fiu.edu (S.H.); ichakrab@fiu.edu (I.C.)

\* Correspondence: mebel@fiu.edu (A.M.M.); rraptis@fiu.edu (R.G.R.)

**Abstract:** Prior to 2021, 4-bromo-1*H*-pyrazole (published in 1999) was the only structurally characterized 4-halogenated-1*H*-pyrazole in the Cambridge Crystallographic Data Center (CCDC). The structures of 4-chloro-1*H*-pyrazole and 4-fluoro-1*H*-pyrazole were published in 2021 and 2023, respectively. Herein, we report the crystal structure for 4-iodo-1*H*-pyrazole, completing the crystallographic data for the series of 4-halogenated-1*H*-pyrazoles. The bromo and chloro analogs are isostructural, forming trimeric H-bonding motifs, whereas the fluoro and iodo analogs form non-isostructural catemers. We also compare the experimental and theoretical (by DFT calculations) IR and <sup>1</sup>H NMR spectroscopic data of the four halogenated 4-X-pzH compounds and unsubstituted pyrazole (pzH). An explanation is offered for some counterintuitive structural, infrared, and <sup>1</sup>H-NMR spectroscopic data.

**Keywords:** pyrazoles; DFT calculations; low temperature



**Citation:** Rue, K.L.; Herrera, S.; Chakraborty, I.; Mebel, A.M.; Raptis, R.G. Completion of Crystallographic Data for the Series of 4-Halogenated-1*H*-pyrazoles: Crystal Structure Determination of 4-Iodo-1*H*-pyrazole and Spectroscopic Comparison. *Crystals* **2023**, *13*, 1101. <https://doi.org/10.3390/cryst13071101>

Academic Editor: Ana M. Garcia-Deibe

Received: 27 June 2023  
 Revised: 10 July 2023  
 Accepted: 12 July 2023  
 Published: 14 July 2023



**Copyright:** © 2023 by the authors. Licensee MDPI, Basel, Switzerland. This article is an open access article distributed under the terms and conditions of the Creative Commons Attribution (CC BY) license (<https://creativecommons.org/licenses/by/4.0/>).

## 1. Introduction

Pyrazoles are five-membered,  $\pi$ -excess heterocycles consisting of three carbon atoms and two adjacent nitrogen atoms (Figure 1). One nitrogen atom (N1) is pyrrole-like while the other (N2) is pyridine-like, allowing for both proton donor and acceptor properties. When N1 is protonated, pyrazole coordinates to metals through N2 as a monodentate ligand; however, N1 is readily deprotonated to form the pyrazolide ion, which can coordinate to metals in an exo- or endo-bidentate fashion in addition to monodentate coordination. The Lewis base tunability (via peripheral substitution) and structural rigidity of the pyrazole ligand led to its extensive applications in coordination chemistry [1–3], while the existence of both donor and acceptor sites in the same molecule enabled its role in supramolecular chemistry [4–8].

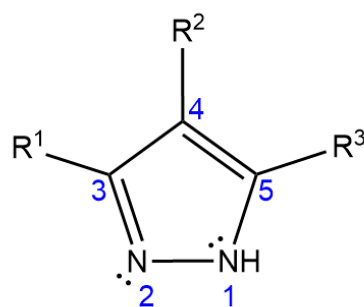


**Figure 1.** Line drawing and numbering scheme of pyrazole backbone.

Pyrazoles can be substituted in the 3-, 4-, and 5-positions while maintaining the ability to form an N(H) ... N hydrogen bonding network involving two or more molecules. The

nature (e.g., electronic and steric properties) and position of the substituents leads to the formation of various H-bonding motifs, such as dimers, trimers, tetramers, and catemers (Figure 2). Attempts were made to derive an empirical rule to predict H-bonding motifs of substituted pyrazoles [9–11], as understanding H-bonding is pertinent for drug design and pyrazoles serve as scaffolds for many biologically active compounds [12–15]. Thus far, it is agreed upon that the four common H-bonding motifs can be classified into two groups—dimers/tetramers and trimers/catemers. Infantes and Motherwell successfully predicted the H-bonding motif of substituted pyrazoles into one of the groups based on the accessible surface of the nitrogen atoms [9]; however, further prediction within each group is still not possible, largely due to limited crystallographic data.

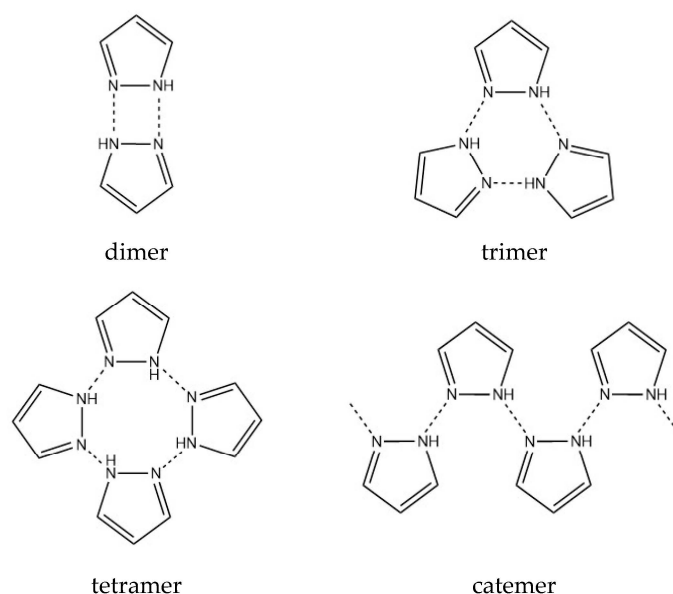


**Figure 2.** Common supramolecular motifs of *1H*-pyrazoles including dimer, trimer, tetramer, and catemer.

The crystal structure of 4-bromo-*1H*-pyrazole (4-Br-pzH) was published in 1999 [16], 4-chloro-*1H*-pyrazole (4-Cl-pzH) in 2021 [17], and, most recently, 4-fluoro-*1H*-pyrazole (4-F-pzH) in 2023 [18]. The bromo and chloro analogs are isostructural and form trimeric H-bonding motifs; however, the fluoro analog forms catemeric chains. Herein, we report the crystal structure for 4-iodo-*1H*-pyrazole (4-I-pzH), completing the crystallographic data for the series of 4-*X*-*1H*-pyrazoles (4-*X*-pzH, where *X* = F, Cl, Br, I). Like 4-F-pzH, the iodo analog forms a catemeric H-bonded motif but, unlike the chloro and bromo analogs, 4-F-pzH and 4-I-pzH are not isostructural. We also compare experimental and computational spectroscopic data of the halogenated 4-*X*-pzH analogs and the unsubstituted pyrazole (pzH).

## 2. Materials and Methods

### 2.1. Materials

All pyrazoles, except for 4-F-pzH, were obtained commercially; 4-F-pzH was received as a gift from Prof. Gellert Mezei, University of Western Michigan. Crystals of 4-I-pzH were present in the commercial bottle via sublimation. <sup>1</sup>H NMR and solid state infrared spectra were recorded on a 400 MHz Bruker Avance NMR spectrometer and an Agilent Advanced Cary-660 FT-IR spectrometer, respectively.

### 2.2. DFT Calculations

Geometry optimization of the structures of pyrazole and its halogen-substituted analogues in the gas phase was carried out within density functional theory (DFT) using the  $\omega$ B97XD [19] hybrid density functional with Dunning's correlation-consistent cc-pVTZ

basis set for H, C, N, F, Cl, and Br [20] employing the Gaussian 16 [21] software package. For I, the dhf-ECP small core effective core potential was employed in conjunction with the cc-pVTZ-PP basis set [22]. Calculations of vibrational frequencies were performed at the same level of theory. To ensure a more appropriate comparison with N-H stretching frequencies measured in solids, geometries of H-bonded dimers, as shown in Figure 2, were optimized and their vibrational frequencies were also computed. <sup>1</sup>H NMR chemical shifts for the monomers in solution were carried out using the GIAO approach [23] within the second order Møller–Plessett perturbation theory MP2 [24] with the cc-pVTZ basis set. The dielectric continuum SCRF/PCM approach [25] was used to take solvent effect into account using parameters of dichloromethane as the solvent.

### 2.3. X-ray Crystallography and Data Collection

A suitable crystal of 4-I-pzH, obtained through sublimation, was selected and mounted on a Bruker D8 Quest diffractometer equipped with a PHOTON II detector operating at T = 172 K. Data were collected with the shutterless  $\omega$ -scan technique using graphite monochromated Mo-K $\alpha$  radiation ( $\lambda = 0.71073$  Å). Structure solution was obtained via intrinsic phasing with SHELXT [26] using the APEX 3 suite [27]. Data were then refined, using the Olex2 [28] interface, by least-squares method in SHELXL [29]. Multiscan absorption corrections were applied and hydrogen atoms were added using the AFIX command. Crystal data and structure refinement parameters are listed in Table 1. Geometric parameters were calculated using Mercury [30] software and the Olex2 suite. CCDC 2271964 contains the supplementary crystallographic data and can be obtained free of charge from the Cambridge Crystallographic Data Center via [www.ccdc.cam.ac.uk/data\\_request/cif](http://www.ccdc.cam.ac.uk/data_request/cif).

**Table 1.** Crystal data and structure refinement parameters for 4-I-pzH.

	4-I-pzH
Formula	C <sub>3</sub> H <sub>3</sub> IN <sub>2</sub>
D <sub>calc.</sub> /g cm <sup>-3</sup>	2.571
$\mu$ /mm <sup>-1</sup>	6.23
Formula Weight	193.97
T/K	172
Crystal System	Orthorhombic
Space group	<i>Cmme</i> (No. 67)
a/Å	6.9383 (6)
b/Å	5.5231 (5)
c/Å	13.077 (2)
$\alpha, \beta, \gamma$ /°	90, 90, 90
V/Å <sup>3</sup>	501.13 (8)
Z	4
Wavelength/Å	0.71073
Radiation Type	Mo K $\alpha$
$\theta_{\min}, \theta_{\max}$ /°	3.1, 31.1
Measured Refl.	5294
Independent Refl.	483
R <sub>int</sub>	0.039
Parameters	55
<sup>a</sup> GooF, <sup>b</sup> wR <sub>2</sub> , <sup>c</sup> R <sub>1</sub>	1.20, 0.068, 0.030

<sup>a</sup> GooF =  $\left[ \frac{\sum [w(F_o^2 - F_c^2)^2]}{(N_o - N_v)} \right]^{1/2}$  ( $N_o$  = number of observations,  $N_v$  = number of variables). <sup>b</sup> wR<sub>2</sub> =  $\frac{\sum [w(F_o - |F_c|)]^2}{\sum |F_o|^2}$ . <sup>c</sup> R<sub>1</sub> =  $\left[ \frac{\sum w(F_o^2 - F_c^2)^2}{\sum |F_o|^2} \right]^{1/2}$ .

## 3. Results and Discussion

### 3.1. Crystal Structure Description

Crystals of 4-I-pzH were obtained through sublimation and found to belong in the orthorhombic *Cmme* space group with one-fourth of the molecule in the asymmetric unit (Figure 3a) disordered equally over four positions (Figure 3b) related by a two-fold rotation

parallel to the *c*-axis and a mirror plane perpendicular to the *b*-axis. Whereas PLATON did not suggest a different unit cell, solutions with unit cells with double the *a*- and *b*-axes, which would eliminate the disorder, were nevertheless attempted unsuccessfully. The use of different crystallization methods and solvents did not afford a crystal structure free of crystallographic disorder. Additionally, the N-H proton is tautomericly disordered over two positions. Of the 4-*X*-pzH series, the crystal structure of 4-I-pzH is the only one with disorder (aside from N-H tautomerization) and, hence,  $Z' = 0.25$  ( $Z' = 2$  and  $1.5$  for  $X = \text{F}$  and  $\text{Cl}/\text{Br}$ , respectively). In the *Cmme* space group, the symmetry and proton disorder make determining the H-bonding network crystallographically impossible; therefore, the structure was solved again in lower symmetry space groups. The *P2<sub>1</sub>ab* space group yielded the best refinement that eliminates disorder and allows for discussion of the supramolecular structure; thus, the following structural description of 4-I-pzH refers to the *P2<sub>1</sub>ab* space group solution. Figure 3c shows the thermal ellipsoid plot and numbering scheme of the *P2<sub>1</sub>ab* structure and refinement details can be found in the Supplemental information (Table S1).

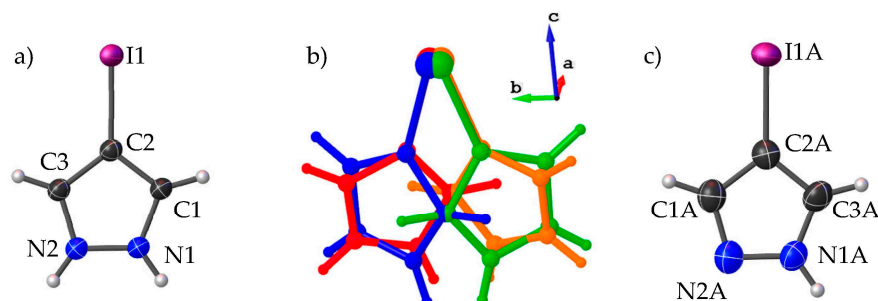


**Figure 3.** (a) Perspective view and numbering scheme of the asymmetric unit of 4-I-pzH in the *Cmme* space group. Thermal ellipsoids are shown at 50% probability. The N-H proton is disordered over two positions and the entire molecule is additionally disordered over four positions. (b) Positional disorder of 4-I-pzH; the entire molecule of each position is shown in a different color for clarity. (c) Perspective view and numbering scheme of the asymmetric unit of 4-I-pzH in the *P2<sub>1</sub>ab* space group with thermal ellipsoids are shown at 50% probability. There is no positional disorder of the N-H proton or the molecule in this space group.

Like 4-F-pzH [18], 4-I-pzH forms a catemeric H-bonded network that extends along the *a*-axis (Figure 4). However, the fluoro and iodo analogs are not isostructural as the trimeric motifs of 4-Br-pzH [16] and 4-Cl-pzH [17] are. Whereas the 4-I-pzH contains one quarter molecule in the asymmetric unit, 4-F-pzH contains two crystallographically independent molecules free of disorder in the asymmetric unit; yet, both lead to similar supramolecular catemeric motif structures. It should be noted that the parent pyrazole (1H-pyrazole, pzH) also forms a catemeric motif; however, it is vastly dissimilar to the fluoro and iodo analogs and was described in the literature as a helical arrangement [31,32]. The N(H) ... N distance of 2.87 (3) in 4-I-pzH (N1A(H) ... N2A) is comparable to the average corresponding distance of 2.889 (1) Å in 4-F-pzH (N1\_1(H) ... N2\_2 = 2.876 (1) Å and N1\_2(H) ... N2\_1 = 2.902 (1) Å). Counter to chemical intuition, the electronegativity differences among the halogen substituents are not reflected in the H-bonded N(H) ... N distances in the solid state structures of pyrazole and the set of its 4-halogenated derivatives (Table 2). However, the calculated dipole moments of each pyrazole show a correlation to catemer or trimer formation with the former having a dipole moment greater than 2.5 and the latter less than 2.5.

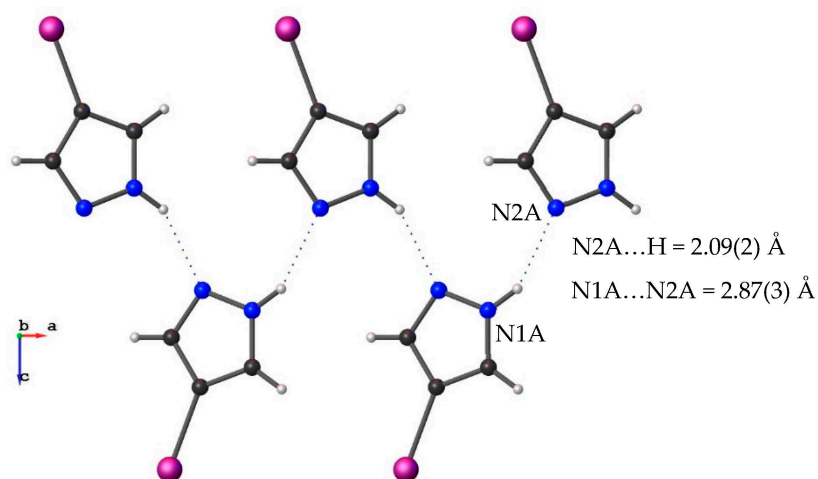


**Figure 4.** H-bonding catemeric motif for 4-I-pzH viewed along the *b*-axis.

**Table 2.** N(H) ... N distances (Å) and calculated dipole moments (D) for pzH and 4-X-pzH (X = F, Cl, Br, I) in relation to crystallographic H-bonding motifs. The average values are given when more than one crystallographically independent N(H) ... N bond exists.

	N(H) ... N	Dipole Moment	Motif	Reference
pzH	2.908 (2)	2.2923	Catemer	[33]
4-F-pzH	2.889 (1)	2.3995	Catemer	[18]
4-Cl-pzH	2.867 (3)	2.5421	Trimer	[17]
4-Br-pzH	2.89 (2)	2.5158	Trimer	[16]
4-I-pzH	2.87 (3)	2.4155	Catemer	This work

The dihedral angle between H-bonded 4-I-pzH planes of  $41.85 (7)^\circ$  is smaller than the dihedral angle of  $59.74 (3)^\circ$  reported for 4-F-pzH; the herringbone motifs of 4-F-pzH and 4-I-pzH, viewed along the *c*-axis, show that the kinks of the former are sharper (Figure 5). While there are C-H- $\pi$  interactions with H ... centroid distances of  $2.72 (1) \text{ \AA}$  and  $3.29 (1) \text{ \AA}$ , the structure of 4-I-pzH has no significant  $\pi$ - $\pi$  interactions (Figure 6).

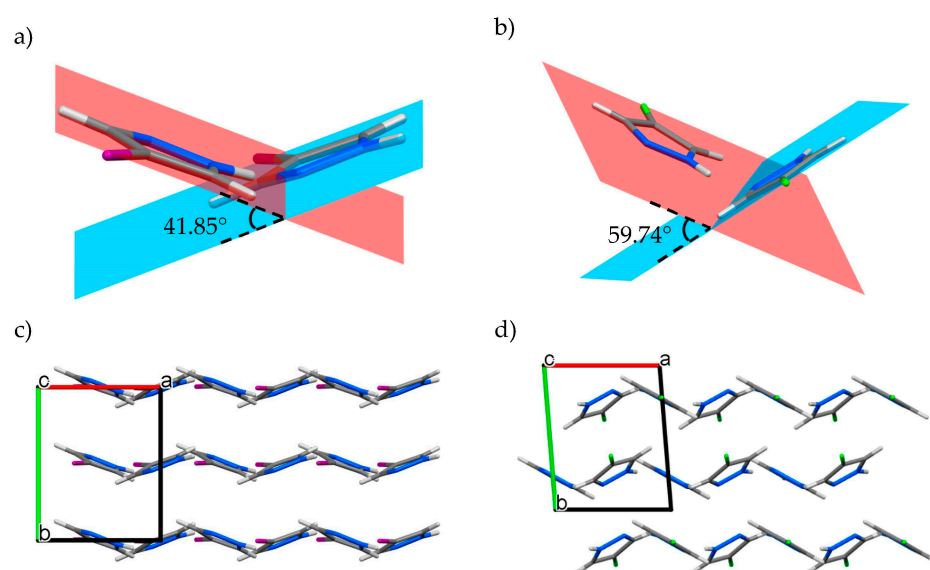


**Figure 5.** Perspective view of the dihedral angle between H-bonded molecules for (a) 4-I-pzH and (b) 4-F-pzH where each plane contains atoms of five-membered heterocycle. Crystal packing, showing the herringbone motif, viewed along the *c*-axis for (c) 4-I-pzH and (d) 4-F-pzH.

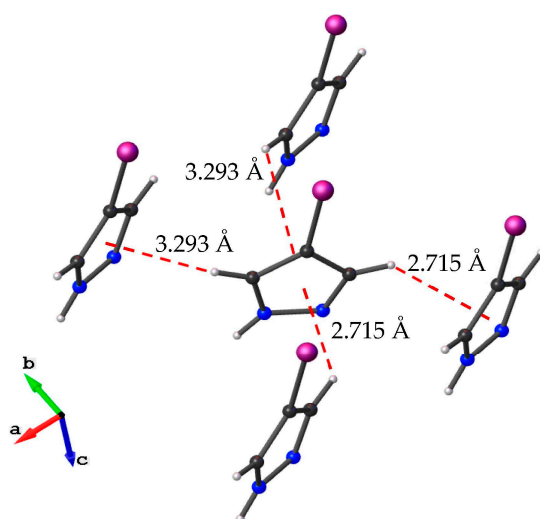


**Figure 6.** Perspective view of C–H– $\pi$  interactions for 4-I-pzH. Distances shown are from the CH proton to the centroid of the plane containing the pyrazole ring.

Halogen bonding interactions exert weak intermolecular forces that often determine supramolecular structure with implications manifested in medicinal chemistry, luminescence, gas sorption, crystal engineering, and organic synthesis. Research into the nature of these interactions has been of recent interest [34]. It has been shown that the importance of halogen bonding increases with increasing polarizability of the halogen (i.e.,  $F < Cl < Br < I$ ) [35]. This is illustrated by the shortest  $X \dots X$  distances of the 4-F-pzH and 4-I-pzH crystal structures: while the  $I \dots I$  closest distance (3.9671 (15) Å) is roughly twice the van der Waals radius (1.98 Å [36]), the closest  $F \dots F$  interaction (3.0270 (9) Å) is significantly longer than twice the van der Waals radius (1.47 Å [36]).  $X \dots X$  interactions are also present in the 4-Cl-pzH and 4-Br-pzH structures with the shortest  $Cl \dots Cl$  distance of 3.7937 (4) Å and  $Br \dots Br$  distance of 3.9103 (9) Å, each of which is slightly larger than twice the van der Waals radius reported by Bondi [36].

The  $F \dots F$  distances between neighboring molecules of the 4-F-pzH range from 3.0270 (9) Å to 5.6045 (2) Å (Figure S1a), while the corresponding  $I \dots I$  distances of 4-I-pzH range from 3.9671 (15) Å to 5.5309 (6) Å (Figure S1b). Figure 7 shows differences in  $I \dots I$  and  $F \dots F$  interactions viewed perpendicularly to the  $c$ -axis. In 4-I-pzH, the I atom of one molecule is exactly centered among the four I atoms of four adjacent molecules with I-to-plane distance of 2.844 (2) Å. Similarly, each F atom of one 4-F-pzH molecule is approximately centered among the F atoms of three neighboring molecules. The distance between F1\_1 and plane [F1\_1 F1\_2 F1\_2] is 1.0881 (8) Å, while the distance between F1\_1 and the centroid of the same plane is 1.394 (1) Å, giving an off-center distance of 0.871 (1) Å. The distance between F1\_2 and plane [F1\_1 F1\_1 F1\_2] is 0.362 (1) Å, while the distance between F1\_2 and the centroid of the same plane is 0.468 (1) Å, giving an off-center distance of 0.296 (1) Å.

C–X bond lengths were analyzed for the series of 4-halogenated pyrazoles and compared with the sum of covalent radii [37] for the respective C–X bonds (Table 3). The C–F bond is statistically longer than the sum of covalent radii, while the C–Cl, C–Br, and C–I bond lengths are increasingly shorter, suggesting a partial C–X double bond for  $X = Cl, Br, \text{ and } I$ , resulting from the overlap of filled halogen p-orbitals with vacant  $\pi^*$ -pzH.

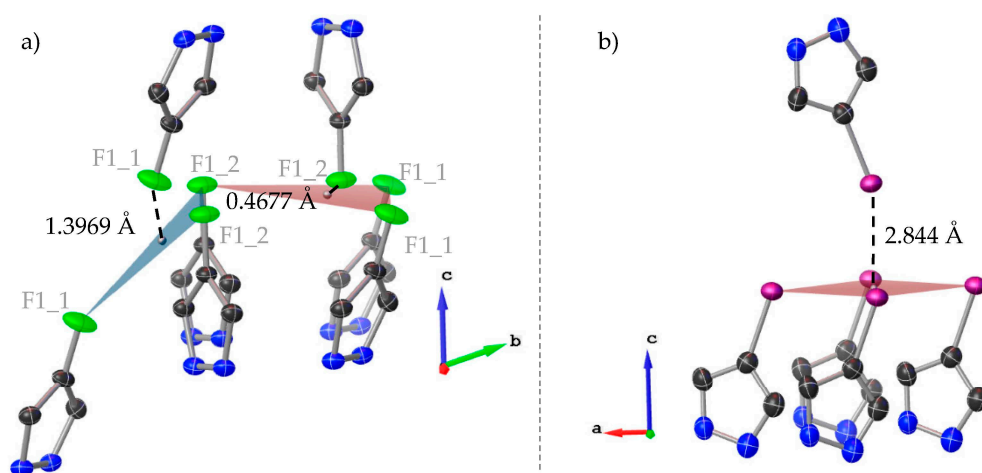


**Figure 7.** Halide to halide plane interactions shown parallel to the *c*-axis for (a) 4-F-pzH and (b) 4-I-pzH. The halide to plane centroid distances are displayed. Hydrogen atoms have been removed for clarity.

**Table 3.** Sum of covalent radii and average C–X bond lengths taken from crystal data.

	C–X Bond Length (Å)	Sum of C–X Covalent Radii (Å) [37]	Difference (Experimental—cov. Radii, Å)
4-F-pzH	1.341(2)	1.30(4)	0.04
4-Cl-pzH	1.717(3)	1.75(4)	−0.02
4-Br-pzH	1.874(11)	1.93(4)	−0.06
4-I-pzH	2.039(9)	2.12(4)	−0.08

### 3.2. Spectroscopy and DFT Calculations

Substituents on the pyrazole ring can be used to modulate the acidity of the pyrrole-like NH group [38]. Counterintuitively, it has been shown that electron-donating peripheral substituents increase the N–H acidity of pyrazoles [39,40] corresponding to a decrease in infrared N–H stretching frequency and a downfield shift in  $^1\text{H}$ -NMR. The series of 4-halogenated pyrazoles follow this trend with the most electronegative substituent, F, exhibiting the highest N–H stretching frequency in IR and the most upfield chemical shift in NMR; the least electronegative substituent, I, exhibited the opposite effect. While the substituent effect of aromatics have been studied (with benzene having been studied most extensively), the focus of papers has been on how halogens (usually represented by only Cl or Br) relate to other electron donating substituents, or how changing the position of a halide in relation to another substituent on the ring affects aromaticity [41–46]. To the best of our knowledge, the spectroscopy for a full series of halogenated pyrazoles has not been studied.

The infrared spectra of pzH and the series of 4-X-pzH (Figure 8 and Table 3) feature a complex region between 2600 and 3200  $\text{cm}^{-1}$  (Figure S2 shows the spectra with all peaks labeled). While calculations of pyrazole monomers show the NH stretching frequency to be ca. 3400–3500  $\text{cm}^{-1}$ , the presence of H-bonding decreases the frequency of this vibration and gives rise to Fermi resonance interactions and overlap with C–H stretching frequencies [47–49]. The N–H vibrations for H-bonded pyrazole trimers appear at lower energies than those of dimers, which in turn appear at lower energies than those of monomers. IR spectra were recorded in the 4000–600  $\text{cm}^{-1}$  range and the highest stretching frequency seen was a small, barely perceptible, shoulder at 3293, 3288, 3284, 3255, and 3235  $\text{cm}^{-1}$  for the H, F, Cl, Br, and I substituents, respectively. There is a three-component band between 3100 and 3180  $\text{cm}^{-1}$  associated with N–H stretching for each pyrazole (except 4-I-pzH, where the spectrum is not as resolved) as presented in Table 4. Interestingly, the band shape in this region is distinct between trimeric and catemeric motifs. A sharp feature is observed

for the pyrazoles that form catemers at 3126, 3133, and 3110  $\text{cm}^{-1}$  for pzH, 4-F-pzH, and 4-I-pzH, respectively.

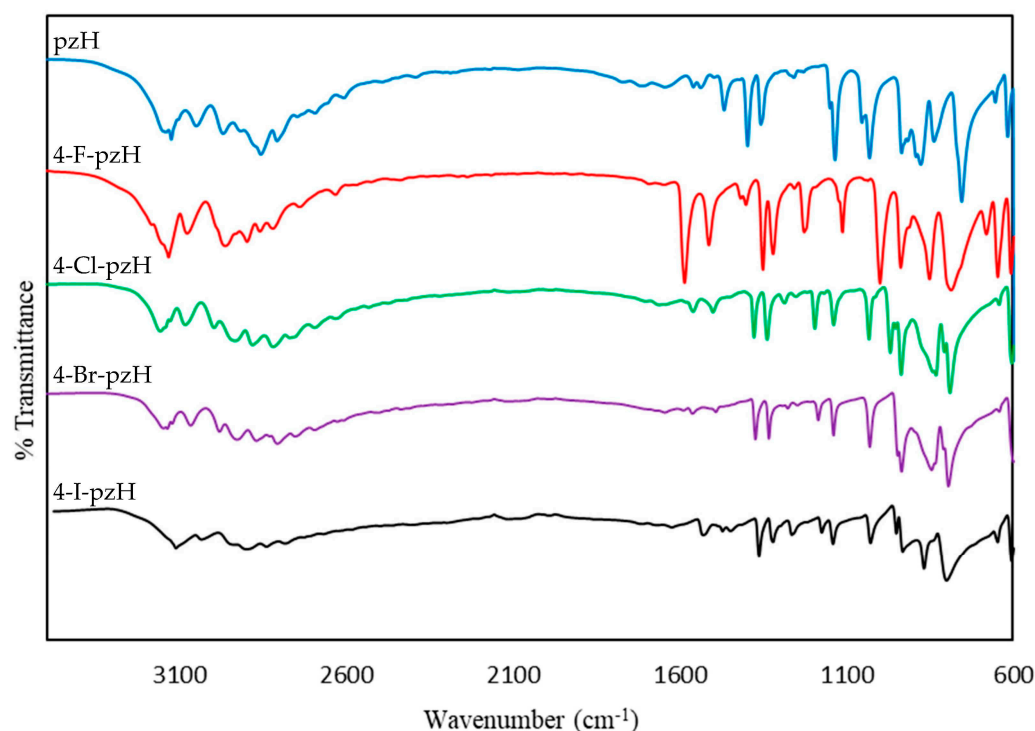


**Figure 8.** Stacked IR spectra of pzH (blue), 4-F-pzH (red), 4-Cl-pzH (green), 4-Br-pzH (purple), and 4-I-pzH (black) from 4000–600  $\text{cm}^{-1}$ .

**Table 4.** Experimental and calculated values for pure N-H solid state stretching modes for pzH and 4-X-pzH. Calculations were carried out using dimeric models; therefore, two distinct stretching frequencies are present.

	Experimental N-H Stretching Modes ( $\text{cm}^{-1}$ )			Calculated N-H Stretching Modes ( $\text{cm}^{-1}$ )	
pzH	3153.04	3126.05	3104.83	3286.3	3265.4
4-F-pzH	3187.76	3154.97	3133.76	3291.2	3270.3
4-Cl-pzH	3156.90	3143.40	3127.97	3286.7	3266.9
4-Br-pzH	3153.04	3137.62	3122.19	3284.9	3265.4
4-I-pzH	-	-	3110.62	3283.2	3264.2

DFT calculations for  $^1\text{H}$  NMR show that the resonances of the N-H proton shift downfield with decreasing electronegativity of the halogen substituent (i.e., fluoro is the further upfield) with values of 9.47 (F), 9.78 (Cl), 9.88 (Br), and 10.00 ppm (I). This trend is observed also in the experimental data (with the exception of a small inversion between 4-Br-pzH and 4-Cl-pzH) with resonances corresponding to the N-H proton at 11.1370 (F), 11.5699 (Cl), 11.5303 (Br), and 11.7549 ppm (I). However, the experimental and theoretical shifts differed by 1.20–1.75 ppm, with the difference attributed to tautomerization, which cannot be modeled by computational methods and imperfect modeling of solvent effects. Tautomerization in solution involving the N-H protons, along with unresolved coupling to quadrupolar N-atom, is responsible also for the broadening of these resonances. DFT calculations predict that the 3,5-protons for 4-F-pzH should be the most upfield, matching the experimental results. Calculations also predict that the Cl, Br, and I analogs should exhibit approximately the same chemical shift (7.63, 7.64, and 7.64 ppm, respectively). However, a small downfield shift was experimentally determined from 4-Cl-pzH to 4-I-pzH. Lastly, DFT predicts that the 3,5-protons of simple pyrazole will be the most downfield;

however, it is observed to be ca. 0.03 ppm upfield of 4-I-pzH. The  $^1\text{H}$  NMR spectra of five compounds are compiled in Figure 9, while experimental and calculated  $^1\text{H}$  NMR data are listed in Table 5. The NMR data are in agreement with those previously published for 4-halopyrazoles [50–52]. Full NMR spectra for each pyrazole can be viewed in the Supplementary information (Figures S3–S7).

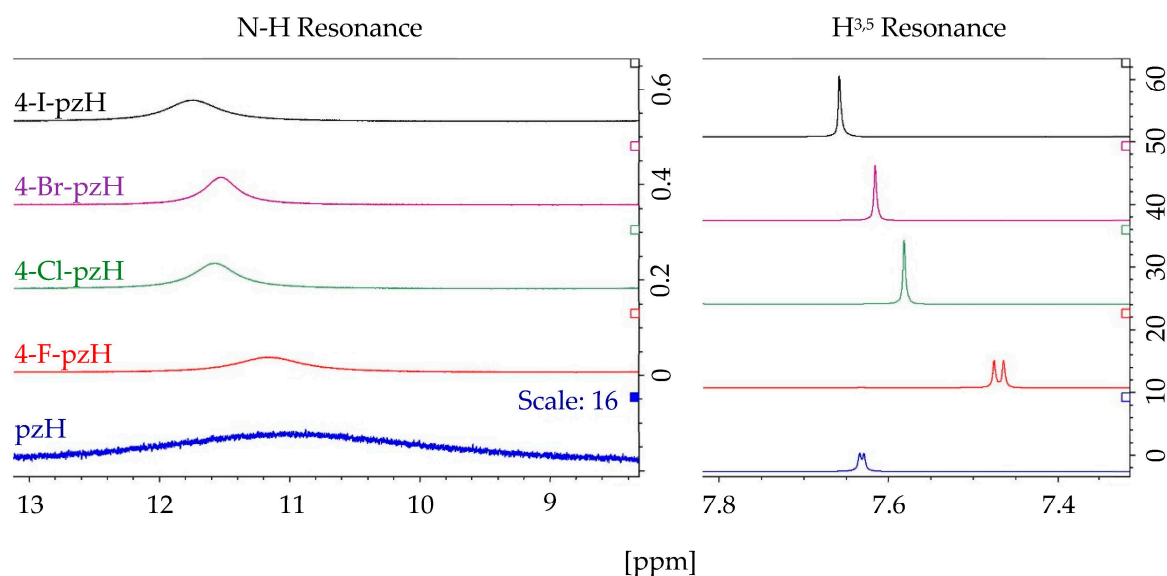


**Figure 9.** Stacked 400 MHz  $^1\text{H}$  NMR spectra in  $\text{CD}_2\text{Cl}_2$  of pzH (blue), 4-F-pzH (red), 4-Cl-pzH (green), 4-Br-pzH (purple), and 4-I-pzH (black). (**Left**): resonances from the N-H proton shown from ~13–8 ppm, scaled by a factor of 100 in relation to the  $\text{H}^{3,5}$  proton resonances. The pzH spectrum is additionally scaled by a factor of 16 to show the N-H resonance. (**Right**): resonances from the  $\text{H}^{3,5}$  proton shown from ~7.8 to 7.5 ppm. All spectra are scaled equally.

**Table 5.**  $^1\text{H}$  NMR experimental data for pzH and 4-X-pzH. Calculated chemical shifts for solutions using the mp2/cc-pVTZ basis set are shown in parentheses.

		N-H	$\text{H}^{3,5}$ <sup>a</sup>	$\text{H}^4$
pzH	Chemical Shift (ppm)	11.087 (9.89)	7.631 (7.74)	6.358 (6.56)
	Multiplicity	s	d	t
	J (Hz)	-	2.1	2.1
	Integration	- <sup>b</sup>	2H	1H
4-F-pzH	Chemical Shift (ppm)	11.137 (9.47)	7.469 (7.52)	-
	Multiplicity	s	d	-
	J (Hz)	-	4.5	-
	Integration	1H	2H	-
4-Cl-pzH	Chemical Shift (ppm)	11.570 (9.78)	7.581 (7.63)	-
	Multiplicity	s	s	-
	J (Hz)	-	-	-
	Integration	1H	2H	-
4-Br-pzH	Chemical Shift (ppm)	11.530 (9.88)	7.615 (7.64)	-
	Multiplicity	s	s	-
	J (Hz)	-	-	-
	Integration	1H	2H	-

Table 5. Cont.

		N-H	H <sup>3,5</sup> <sup>a</sup>	H <sup>4</sup>
4-I-pzH	Chemical Shift (ppm)	11.755 (10.00)	7.658 (7.64)	-
	Multiplicity	s	s	-
	J (Hz)	-	-	-
	Integration	1H	2H	-

<sup>a</sup> Calculated chemical shift is an average of values for protons in the 3 and 5 positions; at room temperature, these protons are equivalent due to tautomerization. <sup>b</sup> Integration for the N-H proton in pzH is not accurate as this proton undergoes fast exchange and is broadened more than the halogenated pyrazoles.

#### 4. Conclusions

With the crystal structure determination of 4-I-pzH, the crystallographic data of the series of 4-halo-1*H*-pyrazoles is now complete. The packing motifs of 4-Cl-pzH and 4-Br-pzH are isostructural and form trimeric units; however, 4-F-pzH and 4-I-pzH both form catemeric structures, but are not isostructural. In spite of the electronegativity difference between 4-F and 4-I substituents, the intermolecular H-bonded N...N distances are indistinguishable within experimental error. The acidity increased from 4-F-pzH to 4-I-pzH, observed in both the trend of infrared N-H stretching modes and <sup>1</sup>H-NMR shifts, are also counterintuitive, but nevertheless modeled by DFT calculations. We propose that these trends are attributed to a partial C-X double bond formation of increasing importance for the heavier halogens, which increases the sp<sup>2</sup> rather than sp<sup>3</sup> hybridization of the N-atom, thus increasing its acidity.

**Supplementary Materials:** The following supporting information can be downloaded at: <https://www.mdpi.com/article/10.3390/cryst13071101/s1>, Table S1: Crystal data refinement parameters for 4-I-pzH in the P21ab space group; Figure S1: Perspective view showing nearest neighbors of the central molecule (black) for (a) 4-F-pzH and (b) 4-I-pzH. Individual molecules and their corresponding distance from the central molecule are color coded to match; Figure S2: Annotated IR spectra of simple pyrazole and 4-X-pyrazole (where X = F, Cl, Br, I); Figure S3: Full 400 MHz <sup>1</sup>H NMR spectrum of 4-F-pyrazole in CD<sub>2</sub>Cl<sub>2</sub>; Figure S4: Full 400 MHz <sup>1</sup>H NMR spectrum of 4-F-pyrazole in CD<sub>2</sub>Cl<sub>2</sub>; Figure S5: Full 400 MHz <sup>1</sup>H NMR spectrum of 4-Cl-pyrazole in CD<sub>2</sub>Cl<sub>2</sub>; Figure S6: Full 400 MHz <sup>1</sup>H NMR spectrum of 4-Br-pyrazole in CD<sub>2</sub>Cl<sub>2</sub>; Figure S7: Full 400 MHz <sup>1</sup>H NMR spectrum of 4-I-pyrazole in CD<sub>2</sub>Cl<sub>2</sub>. The cif and checkcif were provided in the supplementary material.

**Author Contributions:** K.L.R., investigation, data analysis, manuscript preparation; S.H., investigation, data analysis; I.C., data analysis; A.M.M., computational DFT data; R.G.R., supervision, manuscript preparation. All authors have read and agreed to the published version of the manuscript.

**Funding:** K.L.R. was supported by U.S. Nuclear Regulatory Commission (NRC) fellowship grant No. 31310018M0012 awarded to FIU.

**Data Availability Statement:** Not applicable.

**Acknowledgments:** The authors would like to acknowledge Gellert Mezei for a gift of 4-F-pzH and Matthias Zeller for helpful crystallography discussion.

**Conflicts of Interest:** The authors declare no conflict of interest.

#### References

1. Trofimenko, S. Coordination Chemistry of Pyrazole-Derived Ligands. *Chem. Rev.* **1972**, *72*, 497–509. [CrossRef]
2. Viciano-Chumillas, M.; Tanase, S.; de Jongh, L.J.; Reedijk, J. Coordination Versatility of Pyrazole-Based Ligands towards High-Nuclearity Transition-Metal and Rare-Earth Clusters. *Eur. J. Inorg. Chem.* **2010**, *2010*, 3403–3418. [CrossRef]
3. La Monica, G.; Ardizzoia, G.A. The Role of the Pyrazolate Ligand in Building Polynuclear Transition Metal Systems. In *Progress in Inorganic Chemistry*; Karlin, K.D., Ed.; John Wiley & Sons, Inc.: Hoboken, NJ, USA, 2007; pp. 151–238. [CrossRef]
4. Pérez, J.; Riera, L. Pyrazole Complexes and Supramolecular Chemistry. *Eur. J. Inorg. Chem.* **2009**, *2009*, 4913–4925. [CrossRef]
5. Song, X.; Wang, Y.; Wang, C.; Wang, D.; Zhuang, G.; Kirlikovali, K.O.; Li, P.; Farha, O.K. Design Rules of Hydrogen-Bonded Organic Frameworks with High Chemical and Thermal Stabilities. *J. Am. Chem. Soc.* **2022**, *144*, 10663–10687. [CrossRef]
6. Wang, J.; Zhao, L.-R.; Tong, J.; Yu, Y.-M.; Wang, X.-Y.; Yu, S.-Y. Supramolecular Hydrogen Bonding Assembly from Non-Coplanar Aromatic Tetra-<sup>1</sup>H-Pyrazoles with Crystallization-Induced Emission (CIE). *Int. J. Mol. Sci.* **2022**, *23*, 4206. [CrossRef]

7. Brewer, G.; Butcher, R.J.; Zavalij, P. Use of Pyrazole Hydrogen Bonding in Tripodal Complexes to Form Self Assembled Homochiral Dimers. *Materials* **2020**, *13*, 1595. [CrossRef]
8. Moyano, S.; Diosdado, B.; Felices, L.S.; Elduque, A.; Giménez, R. Structural Diversity of Hydrogen-Bonded 4-Aryl-3,5-Dimethylpyrazoles for Supramolecular Materials. *Materials* **2021**, *14*, 4550. [CrossRef]
9. Infantes, L.; Motherwell, S. Prediction of H-Bonding Motifs for Pyrazoles and Oximes Using the Cambridge Structural Database. *Struct. Chem.* **2004**, *15*, 173–184. [CrossRef]
10. Alkorta, I.; Elguero, J.; Foces-Foces, C.; Infantes, L. Classification of hydrogen-bond motives in crystals of NH-pyrazoles: A mixed empirical and theoretical approach. *Arkivoc* **2005**, *2006*, 15–30. [CrossRef]
11. Foces-Foces, C.; Alkorta, I.; Elguero, J. Supramolecular Structure of 1H-Pyrazoles in the Solid State: A Crystallographic and Ab Initio Study. *Acta Crystallogr. Sect. B Struct. Sci.* **2000**, *56*, 1018–1028. [CrossRef]
12. Karrouchi, K.; Radi, S.; Ramli, Y.; Taoufik, J.; Mabkhot, Y.N.; Al-Aizari, F.A.; Ansar, M. Synthesis and Pharmacological Activities of Pyrazole Derivatives: A Review. *Molecules* **2018**, *23*, 134. [CrossRef]
13. Ansari, A.; Ali, A.; Asif, M.; Shamsuzzaman, S. Biologically Active Pyrazole Derivatives. *New J. Chem.* **2017**, *41*, 16–41. [CrossRef]
14. Li, G.; Cheng, Y.; Han, C.; Song, C.; Huang, N.; Du, Y. Pyrazole-Containing Pharmaceuticals: Target, Pharmacological Activity, and Their SAR Studies. *RSC Med. Chem.* **2022**, *13*, 1300–1321. [CrossRef]
15. Elkanzi, N.A.A.; Zahou, F.M. Short Review on Pharmacological Characteristics and Synthesis of Pyrazole. *Heterocycl. Lett.* **2021**, *11*, 111–130.
16. Foces-Foces, C.; Llamas-Saiz, A.L.; Elguero, J. Crystal Structures of Two 4-Bromopyrazole Derivatives. *Z. Kristallogr. Cryst. Mater.* **1999**, *214*, 237–241. [CrossRef]
17. Rue, K.; Raptis, R.G. Low-Temperature Crystal Structure of 4-Chloro-1 H -Pyrazole. *Acta Crystallogr. E Cryst. Commun.* **2021**, *77*, 955–957. [CrossRef]
18. Ahmed, B.M.; Zeller, M.; Mezei, G. Crystal and Molecular Structure of 4-Fluoro-1 H -Pyrazole at 150 K. *Acta Crystallogr. E Cryst. Commun.* **2023**, *79*, 428–431. [CrossRef]
19. Chai, J.-D.; Head-Gordon, M. Long-Range Corrected Hybrid Density Functionals with Damped Atom–Atom Dispersion Corrections. *Phys. Chem. Chem. Phys.* **2008**, *10*, 6615–6620. [CrossRef]
20. Dunning, T.H., Jr. Gaussian basis sets for use in correlated molecular calculations. I. The atoms boron through neon and hydrogen. *J. Chem. Phys.* **1989**, *90*, 1007–1023. [CrossRef]
21. Frisch, M.J.; Trucks, G.W.; Schlegel, H.B.; Scuseria, G.E.; Robb, M.A.; Cheeseman, J.R.; Scalmani, G.; Barone, V.; Petersson, G.A.; Nakatsuji, H.; et al. *GAUSSIAN 16, Revision C.1*; Gaussian Inc.: Wallingford, CT, USA, 2019.
22. Basis Set Exchange Library. Available online: <https://www.basissetexchange.org/> (accessed on 12 June 2023).
23. CCheeseman, J.R.; Trucks, G.W.; Keith, T.A.; Frisch, M.J. A Comparison of Models for Calculating Nuclear Magnetic Resonance Shielding Tensors. *J. Chem. Phys.* **1996**, *104*, 5497–5509. [CrossRef]
24. Frisch, M.J.; Head-Gordon, M.; Pople, J.A. Semi-direct algorithms for the MP2 energy and gradient. *Chem. Phys. Lett.* **1990**, *166*, 281–289. [CrossRef]
25. Tomasi, J.; Mennucci, B.; Cammi, R. Quantum Mechanical Continuum Solvation Models. *Chem. Rev.* **2005**, *105*, 2999–3094. [CrossRef] [PubMed]
26. Sheldrick, G.M. SHELXT—Integrated Space-Group and Crystal-Structure Determination. *Acta Crystallogr. A* **2015**, *71*, 3–8. [CrossRef] [PubMed]
27. Bruker. APEX3; Bruker AXS LLC: Madison, WI, USA, 2020.
28. Dolomanov, O.V.; Bourhis, L.J.; Gildea, R.J.; Howard, J.A.K.; Puschmann, H. OLEX2: A Complete Structure Solution, Refinement and Analysis Program. *J. Appl. Crystallogr.* **2009**, *42*, 339–341. [CrossRef]
29. Sheldrick, G.M. Crystal Structure Refinement with SHELXL. *Acta Crystallogr. C* **2015**, *71*, 3–8. [CrossRef]
30. Macrae, C.F.; Sovago, I.; Cottrell, S.J.; Galek, P.T.A.; McCabe, P.; Pidcock, E.; Platings, M.; Shields, G.P.; Stevens, J.S.; Towler, M.; et al. *Mercury 4.0: From Visualization to Analysis, Design and Prediction*. *J. Appl. Crystallogr.* **2020**, *53*, 226–235. [CrossRef]
31. Ehrlich, H.W. The Crystal and Molecular Structure of Pyrazole. *Acta Crystallogr.* **1960**, *13*, 946–952. [CrossRef]
32. Sikora, M.; Katrusiak, A. Pressure-Controlled Neutral–Ionic Transition and Disordering of NH···N Hydrogen Bonds in Pyrazole. *J. Phys. Chem. C* **2013**, *117*, 10661–10668. [CrossRef]
33. Larsen, F.K.; Lehmann, M.S.; Søtofte, I.; Rasmussen, S.E. A Neutron Diffraction Study of the Crystal and Molecular Structure of Pyrazole, C<sub>3</sub>H<sub>4</sub>N<sub>2</sub>. *Acta Chem. Scand.* **1970**, *24*, 3248–3258. [CrossRef]
34. Saha, B.K.; Veluthaparambath, R.V.; Krishna, G.V. Halogen···Halogen Interactions: Nature, Directionality and Applications. *Chem. Asian J.* **2023**, *18*, e202300067. [CrossRef]
35. Cavallo, G.; Metrangolo, P.; Milani, R.; Pilati, T.; Priimagi, A.; Resnati, G.; Terraneo, G. The Halogen Bond. *Chem. Rev.* **2016**, *116*, 2478–2601. [CrossRef]
36. Bondi, A. Van der Waals Volumes and Radii. *J. Phys. Chem.* **1964**, *68*, 441–451. [CrossRef]
37. Cordero, B.; Gómez, V.; Platero-Prats, A.E.; Revés, M.; Echeverría, J.; Cremades, E.; Barragán, F.; Alvarez, S. Covalent radii revisited. *Dalton Trans.* **2008**, 2832–2838. [CrossRef]
38. Secrieru, A.; O’neill, P.M.; Cristiano, M.L.S. Revisiting the Structure and Chemistry of 3(5)-Substituted Pyrazoles. *Molecules* **2020**, *25*, 42. [CrossRef]

39. Notario, R.; Herreros, M.; El Hammadi, A.; Homan, H.; Abboud, J.-L.M.; Forfar, I.; Claramunt, R.M.; Elguero, J. Similarity in Physical and Organic Chemistry: Substituent Effects on the Intrinsic Basicity of 4-Substituted Pyrazoles. *J. Phys. Org. Chem.* **1994**, *7*, 657–662. [[CrossRef](#)]
40. Catalan, J.; Elguero, J. Basicity and Acidity of Azoles. In *Advances in Heterocyclic Chemistry*; Elsevier: Amsterdam, The Netherlands, 1987; Volume 41, pp. 187–274. [[CrossRef](#)]
41. Gümüş, S.; Türker, L. Substituent effect on the aromaticity of 1,3-azole systems. *Heterocycl. Commun.* **2012**, *18*, 11–16. [[CrossRef](#)]
42. Smith, W.B.; Ihrig, A.M.; Roark, J.L. Substituent Effects on Aromatic Proton Chemical Shifts. VII. Further Examples Drawn from Disubstituted Benzenes. *J. Phys. Chem.* **1970**, *74*, 74812–74821. [[CrossRef](#)]
43. Scheiner, S.; Hunter, S. Influence of Substituents in the Benzene Ring on the Halogen Bond of Iodobenzene with Ammonia. *ChemPhysChem* **2022**, *23*, e202200011. [[CrossRef](#)]
44. Baranac-Stojanović, M. Substituent Effect on the Triplet State Aromaticity of Benzene. *J. Org. Chem.* **2020**, *85*, 4289–4297. [[CrossRef](#)]
45. Palusiak, M.; Domagała, M.; Dominikowska, J.; Bickelhaupt, F.M. The Substituent Effect on Benzene Dications. *Phys. Chem. Chem. Phys.* **2014**, *16*, 4752–4763. [[CrossRef](#)]
46. Abedini, N.; Kassae, M.Z. The Effects of Halogen Substituents on Structure, Stability, and Electronic Properties of bicyclo[1.1.1]pentanylene at Density Functional Theory. *J. Phys. Org. Chem.* **2022**, *35*, e4304. [[CrossRef](#)]
47. Wassermann, T.N.; Rice, C.A.; Suhm, M.A.; Luckhaus, D. Hydrogen Bonding Lights up Overtones in Pyrazoles. *J. Chem. Phys.* **2007**, *127*, 234309. [[CrossRef](#)] [[PubMed](#)]
48. Wolff, H.; Müller, H. Structure of the NH Stretching Vibrational Band of Pyrazole. Multiple Resonance of Substances Forming Strong H or D Bonds. *Spectrochim. Acta Part A Mol. Spectrosc.* **1976**, *32*, 581–585. [[CrossRef](#)]
49. Rice, C.A.; Borho, N.; Suhm, M.A. Dimerization of Pyrazole in Slit Jet Expansions. *Z. Phys. Chem.* **2005**, *219*, 379–388. [[CrossRef](#)]
50. Hanamoto, T.; Koga, Y.; Kido, E.; Kawanami, T.; Furuno, H.; Inanaga, J. Palladium catalyzed cross-coupling reaction of 5-tributylstannyl-4-fluoropyrazole. *Chem. Commun.* **2005**, *15*, 2041–2043. [[CrossRef](#)]
51. Zhao, Z.-G.; Wang, Z.-X. Halogenation of Pyrazoles using N-Halosuccinimides in CCl<sub>4</sub> and in Water. *Synth. Commun.* **2007**, *37*, 137–147. [[CrossRef](#)]
52. Mezei, G.; Raptis, R.G. Effect of Pyrazole-Substitution on the Structure and Nuclearity of Cu(II)-Pyrazolato Complexes. *Inorg. Chim. Acta* **2004**, *357*, 3279–3288. [[CrossRef](#)]

**Disclaimer/Publisher's Note:** The statements, opinions and data contained in all publications are solely those of the individual author(s) and contributor(s) and not of MDPI and/or the editor(s). MDPI and/or the editor(s) disclaim responsibility for any injury to people or property resulting from any ideas, methods, instructions or products referred to in the content.